JOURNAL of POLYTECHNIC

ISSN: 1302-0900 (PRINT), ISSN: 2147-9429 (ONLINE)
URL: http://dergipark.org.tr/politeknik

The effect of scanning strategy on mechanical properties and delamination during brake caliper manufacturing with selective laser melting (SLM)

***Author(s)**: Mehmet ÖZAKINCI[1], Rahmi ÜNAL[2]*

ORCID[1]: 0000-0002-1890-4513

ORCID[2]: 0000-0001-5379-5159

To cite to this article: Özakıncı M. and Ünal R., "The effect of scanning strategy on mechanical properties and delamination during brake caliper manufacturing with selective laser melting (SLM)", ***Journal of Polytechnic***, 27(3): 1129-1140, (2024).

Bu makaleye şu şekilde atıfta bulunabilirsiniz: Özakıncı M. and Ünal R., "The effect of scanning strategy on mechanical properties and delamination during brake caliper manufacturing with selective laser melting (SLM)", ***Politeknik Dergisi***, 27(3): 1129-1140, (2024).

To link to this article: http://dergipark.org.tr/politeknik/archive

DOI: **10.2339/politeknik.1214999**

The Effect of Scanning Strategy On Mechanical Properties and Delamination During Brake Caliper Manufacturing With Selective Laser Melting (SLM)

Highlights

- *Manufacturing of service brake caliper with SLM*
- *Caliper manufacturing with 316L stainless steel material*
- *Effect of chessboard and strip scanning strategies on mechanical properties (yield strength, tensile strength, hardness etc.)*
- *Effect of chessboard and stripe scanning strategies on delamination*
- *Effect of chessboard and stripe scanning strategies on porosity*

Graphical Abstract

Methods resolving the delamination issue observed during the production of a service brake caliper using selective laser melting were studied. In this context, the mechanical characteristics of the manufactured samples were determined by laboratory testing.

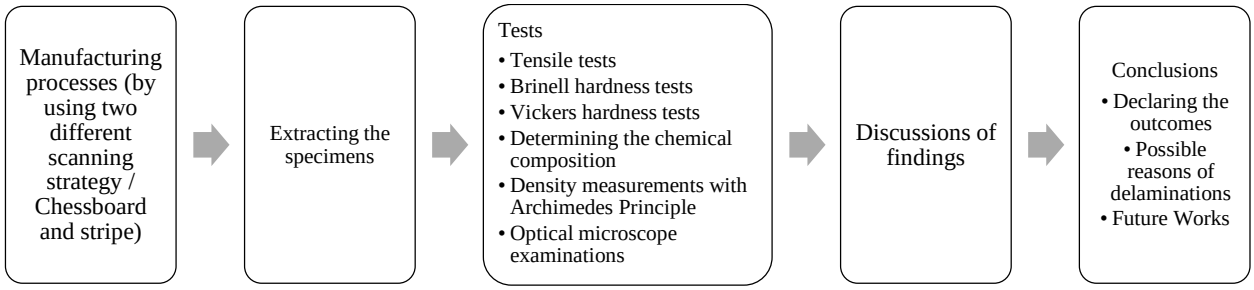

Figure 1. Graphical abstract

Aim

The delamination issue observed during the production of a service brake caliper, from 316L stainless steel using the selective laser melting (SLM) process. The aim of this study is to reveal the causes of delamination and to determine the effect of different screening strategies on mechanical properties.

Design & Methodology

A production study was carried out with different scanning strategies, which are assumed to be the cause/solution of the delamination. Mechanical tests were planned and applied on parts manufactured with different scanning strategies.

Originality

The work of manufacturing the service brake caliper from 316L material with additive manufacturing is an original work. In addition, it is unique that the chessboard method and the stripe method are researched on samples produced in scope of the same study using 316L material.

Findings

According to the findings, the mechanical properties of the parts produced with chessboard are better than those produced with the stripe method. The properties obtained are yield-tensile stress, ductility, hardness, porosity ratios.

Conclusion

Although the formation of delamination is a phenomenon caused by temperature differences and residual stresses reported in the literature, large porosities that occur in the layers during the processing of the part can cause delamination in the upper layers.

Declaration of Ethical Standards

The author(s) of this article declare that the materials and methods used in this study do not require ethical committee permission and/or legal-special permission.

The Effect of Scanning Strategy On Mechanical Properties and Delamination During Brake Caliper Manufacturing With Selective Laser Melting (SLM)

Research Article

Mehmet ÖZAKINCI[1*], Rahmi ÜNAL[2]

[1]FNSS, Ankara-Turkey, FNSS Savunma Sistemleri A.Ş., Oğulbey, Kumludere Cad No:11, 06830 Gölbaşı, Ankara, Turkey
[2]Gazi University, Faculty of Engineering, Mechanical Engineering Department, 06570 Ankara, Turkey

(Geliş/Received : 05.12.2022 ; Kabul/Accepted : 09.03.2023 ; Erken Görünüm/Early View : 12.05.2023)

ABSTRACT

In the industry, additively manufactured components are becoming more prevalent. Rather than the growth in production of ordinary non-structural components by additive manufacturing, Additive manufacturing's increased safety-critical component production drives this prevalence. Thus, additive manufacturing of the braking system part, a vital subsystem in almost all vehicles, will help spread this manufacturing method. This study investigated the delamination issue noticed during the selective laser melting manufacture of the service brake caliper from 316L stainless steel. All process parameters were kept constant to investigate only the scanning strategy effect on the mechanical properties and delamination. On the samples, density-porosity measurements, tensile and hardness tests, and macrostructure examinations using an optical microscope were conducted. As a consequence of the studies, the chessboard scanning strategy exhibited superior mechanical properties over the stripe scanning strategy. The Chessboard method gave better results by 6% for measuring yield stress and by 12% for measuring Brinell hardness. The delamination was not entirely eliminated by the chessboard scanning strategy; however, it was noticed to be reduced in comparison to the stripe scanning strategy. Possible causes of delamination are discussed with microhardness measurements and optical microscope examinations.

Keywords: SLM (selective laser melting), Delamination, 316L stainless steel, Chessboard Scanning strategy, Stripe Scanning strategy

1. INTRODUCTION

The ASTM F2792 standard divides metal additive manufacturing into two categories: direct energy deposition (DED) and powder bed fusion (PBF). They are classified according on the energy source they use [1]. Selective laser melting is a subcategory of PBF production that uses lasers as its energy source. The SLM method stands out among these techniques because of its broad application and excellent dimensional sensitivity [2] [3]. In the fabrication of safety-critical items, it is the most used additive manufacturing method [4]. However, delamination resulting from high residual stresses caused by not optimizing the manufacturing parameters and porosities in the material structure are the biggest obstacles to the use of these parts. [5]. In addition, the particle size in the material microstructure and the angle of build direction have a high effect on the mechanical properties. Reduction of grain size and the perpendicularity of the forces acting on the part to the build direction have a positive effect on the mechanical properties [6], [7]. High thermal input and rapid cooling conditions can also result in delamination and crack formation between layers. Thermal expansion of the warmer top layer causes loads on the relatively cooled bottom layer. If the loads due to this thermal expansion exceed the yield stress, they cause plastic deformations, and if they exceed the tensile stress, they cause cracks and delamination [8]. The melting of grain boundary phases or carbides in these regions that are heated to temperatures below their melting point can act as crack regions and cause delamination [9]. Additionally, it has been observed that large molten metal particle spatters formed by the agglomeration of micro particles in high-energy input regions have a negative effect on the cooling characteristic and cause delamination [10]. It has been determined that the formation of nano-sized needle grain structures positively affects the mechanical properties of the parts manufactured by the SLM method, and the energy density, which is a result of the laser power and scanning speed, is more dominant than the scanning strategy in the formation of these structures. The particle size decreases with the decrease in laser energy density [11]. On the other hand, Liverani et al. in their study, they reported that the effect of increasing the laser power from 100W to 150W on the yield and tensile stresses was negligible, but there was a 10% increase in the elongation to failure value [12].

The study, which is the subject of the article, focused on revealing the causes of delamination encountered during the manufacturing of a hydraulic service brake caliper intended for use in an armored personnel carrier by the selective laser melting method. The caliper, which is the most important element of the brake system, is a safety critical component and it is crucial that it meets the targeted mechanical properties. 316L stainless steel was chosen as the manufacturing material, taking into account factors such as widespread use, mechanical properties, weldability, cost and resistance to corrosion [6]. Within the scope of the study, hardness measurement, tensile test, microstructure analysis, porosity analysis, density measurement, and material composition measurements

* *Corresponding Author*
e-mail : mehmet.ozakinci@fnss.com.tr

were performed on the samples obtained from the two productions, which were started to be produced in different scanning strategies, but both productions were terminated due to delamination. According to the results of these tests and controls, findings on delamination were revealed and root causes were discussed.

2. MATERIAL and METHOD

This section provides information on the study's methodology and the experimental sample preparation phase.

2.1. Intended Geometry, Fabrication And Process Parameters

Figure 1a depicts the geometry for which brake calculations are produced based on the requirements of the caliper and modeled in light of this information.. The production was continued up to the planes shown in Figure 1 with the stripe and chessboard scanning strategies (SSS and CSS), but the fabrication was not continued due to delamination for both scanning strategy. Figure 2 shows the SSS and CSS schematically. In the scanning strategies applied in scope of the study, each layer was processed by turning it at an angle of 67° compared to the previous layer.

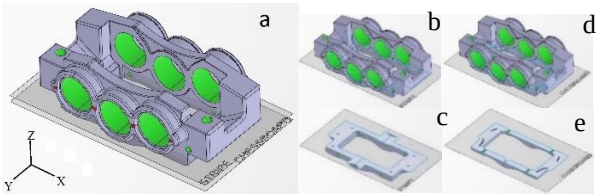

Figure 1. Parts fabricated with the SSS and CSS (c and e). Representation of the planes (a, b and d) on which the production is continued in the part whole

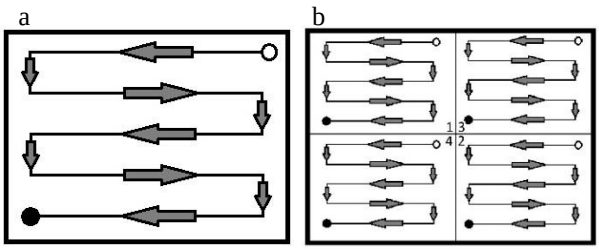

Figure 2. Scanning strategies: (a) the SSS, with each layer rotated 67° in the xy plane, (b) the CSS, with each layer rotated 67° in the xy plane

In the production, the SSS was first used and started with the fabrication of the geometry seen in Figure 1b. However, production was stopped with the observation of delamination. Due to the late detection of delamination during the first production, the parts and samples produced by the SSS are larger than the samples produced by the CSS as can be seen in Figure 1c and Figure 1e. Other photos taken during production can be seen in Figure 4.

Figure 3 depicts the SSS and CSS bodies which production was stopped due to delamination. In addition to the part to be manufactured during the fabrication, the production of three tensile test sample is also planned. Although the production of the parts was stopped, one of the tensile test samples shown in Figure 5 could be produced.

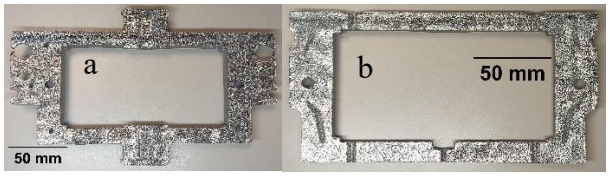

Figure 3. (a) SSS and (b) CSS fabrications

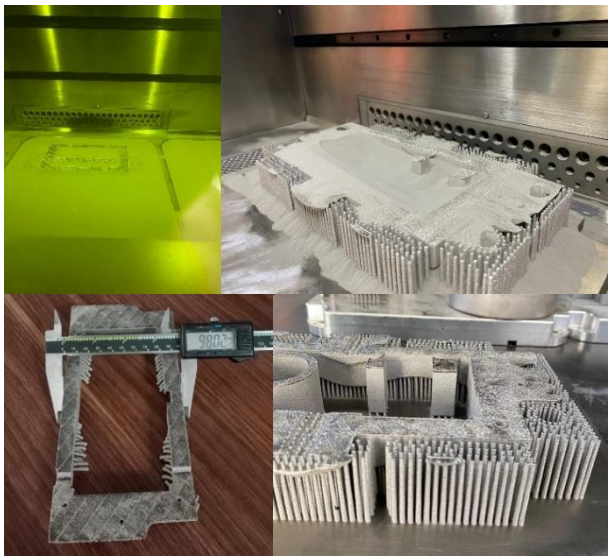

Figure 4. Photos taken during manufacturing

Distortion, cracks, and delamination caused by residual stresses are an important factor preventing the use of metal parts produced with metal additive manufacturing [13]. To prevent or reduce residual stresses, which is one of the main causes of delamination; floor plate preheating, dividing the scanning area into small areas (e.g. CSS) and planning the laser beam movements within these areas, increasing the scanning speed and reducing the layer height can be considered [14]. In the light of this information, after the production with the SSS, the production was repeated with the CSS, keeping all other parameters constant. In repeated production with the CSS, delamination was observed again at a visible level but less than with the SSS. Production could not be continued with this method, and the examination phase, which was the subject of the study, was started. The processing parameters for both productions are shown in **Hata! Başvuru kaynağı bulunamadı.**. In the study, it was aimed to investigate the cause of the delamination in order to determine the correct processing parameters and to complete the production that meets the targeted design with the least production repetition.

Table 1. Process parameters resulting in delamination

Parameter	1. Fabrication	2. Fabrication
Layer thickness (mm)	0,05	0,05
Scanning strategy	Stripe -width: 10 mm	Chess -area: 5 mm X 5 mm
Hatch distance (mm)	0,1	0,1
Scanning start angle (degree)	67	67
Rotation angle per layer (degree)	67	67
Spot size (mm)	0,085	0,085
Laser scanning speed (mm/s)	1100	1100
Laser scanning power (Watt)	370	370

2.2. Tensile Test and Sample Preparation

Tensile test, hardness measurement, macro structure analysis, density measurement, porosity analysis, salt fog test and material composition determination studies were carried out. Sample preparations are very important to determine the cause of delamination in the structure. 2 of each 1 sample with square section, shown in Figure 5, produced with SSS and CSS, 6 mm diameter tensile test samples were produced by machining on a lathe in accordance with ASTM E8 standard (Figure 6) [15] [16]. Figure 8 shows four test specimens for tensile strength. Due to the machinability of 316L stainless steel, the continuous chip formations seen in Figure 5c were obtained, and the machining was completed.

Figure 5. Square cross-section bars produced by the (a) SSS (b) CSS from which the tensile test specimens are obtained. (c) Chips formed in the manufacture of tensile test specimens

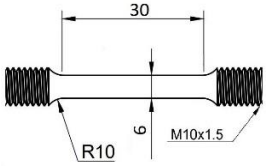

Figure 6. Tensile test specimen dimensions

M10x1.5 thread was drilled on tip of the specimens in order to connect them to the tensile test device. During manual threading, visible discontinuous cracks shown in Figure 7 occurred on the body surface of the cylindrical SSS test specimen due to torsion. Because of this, it was decided that nondestructive testing techniques should be used to examine the surface of the tensile samples. The penetrant test, the results of which can be seen in Figure 8a, was performed by applying fluorescent spray material on the specimens. The dark red areas seen here indicate cracks formed on the surface during the threading of the specimens. In order to determine whether the cracks continued into the body of the specimen, radiographic examination was performed on the Balteau XSD 160 X-Ray imaging device. In the radiography results shown in Figure 8b, no trace of these cracks continuing into the sample body was found.

Figure 7. SSS tensile specimens with surface cracks during threading

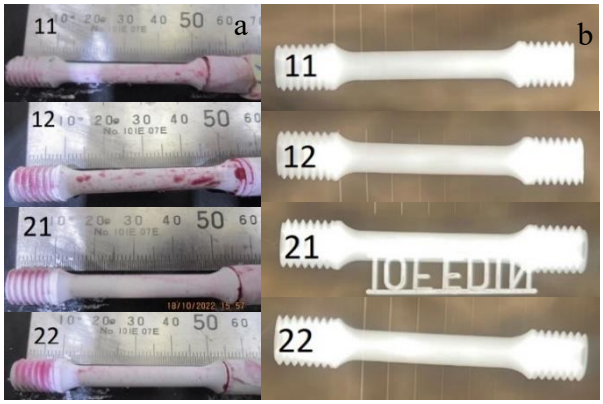

Figure 8. Penetrant test (a) and radiography result (b) photos

The measurement results made in the Zwick/Roell Retroline tensile test equipment. The extensometer connection could not be made due to the insufficient size of the samples. Young's modulus could not be measured for this reason. In addition, the measured elongation values are not exact values and are used for comparison purposes.

2.3. Hardness Measurements

The Brinell hardness test is performed on a polished surface of the test specimen with the proper width and thickness. A polished tungsten carbide ball of a certain diameter is pressed on the test surface with a certain amount of force. The Brinell hardness is proportional to the applied force divided by the indentation's surface area. Test details are available from the ISO 6506-1 standard [17]. The Brinell hardness test results were used to assess the hardness of the samples that were manufactured for the study.

A Vickers low force hardness test (HV 0.5) was performed on SSS and CSS samples obtained from caliper body. Test details are available from the ISO 6507-1 standard [17].

2.4. Definition of Density and Porosity

The densities and porosity ratios of the three samples produced with CSS and SSS were determined according to the Archimedes principle. The samples were obtained by cutting on the lathe from the vertically produced parts seen in Figure 9. The cut samples are numbered 3, 2, and 1 from the bottom layer to the top. The top layers, where delamination of the part was observed, were scrapped up to 3 to 5 mm for both SSS and CSS samples. According to Archimedes' principle, the Equation 1 was used to calculate the density of the samples based on the weight difference between air and distilled water. Details of the principle can be found in the ASTM B311-17 standard [18]. Test equipment for this method can be seen Figure 10.

$$\boldsymbol{D = \frac{AxE}{A-F}} \qquad (1)$$

Where, D is the density of test specimen (g/cm^3), A is the mass of test specimen in the air (g), E is the density of water (g/cm^3), F is the mass of test specimen in water with mass of specimen support tared (g). In order to prevent water ingress into the pores in the pieces for which density measurement was made, they were coated with beeswax [19][20]. The porosity ratios of the samples are calculated as per the formula shown in Equation 2 [21].

$$\boldsymbol{f = 100\left(1 - \frac{D}{D_{th}}\right)} \qquad \boldsymbol{\%D = 100 - f} \qquad (2)$$

Where, f is the porosity ratio, D_{th} is the theoretical density of specimen (8,00 g/cm^3 [22]).

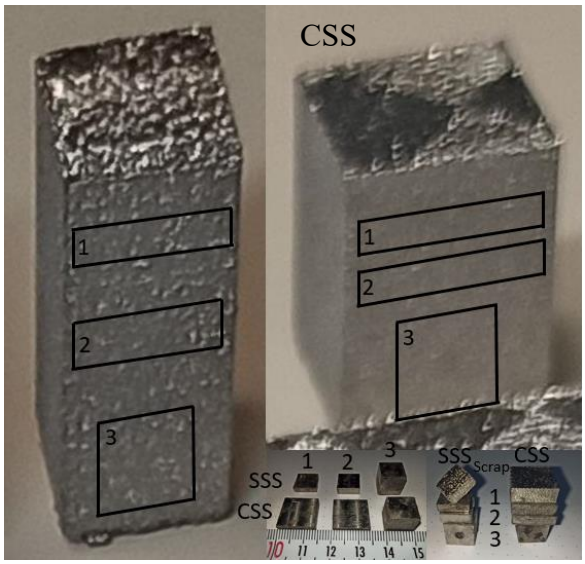

Figure 9. Samples prepared for Archimedes principle

Figure 10. Archimedes' principle test equipment image during sample number ½

2.5. Chemical Composition

The Thermo ARL 3460 Optical Emission Spectrometer was used to determine the chemical composition on the sample fabricated for the study. The measurement results

given in Table 1 were compared with the reference values of EOS Company 316L powder with a 40 µm layer thickness [22]. Accordingly, the material 316L chemical composition is compatible with the reference values.

Table 1. The chemical composition of the sample produced from 316L material, determined by the spectrometer (wt.%)

C	Si	Mn	P	S	Cr	Mo	Ni	Cu	Fe
0,029	0,674	1,482	0,054	0,017	17,256	2,295	12,605	0,062	65,34

2.6. Micro Structural Examinations

5X, 10X, 20X, 50X and 100X magnification rates on a Nikon Eclipse LV150N optical microscope were used to capture pictures for micro structural examination.

3. RESULT AND DISCUSSION

3.1. Volumetric Energy Density

Energy density is a derived parameter that is a function of laser power, layer thickness, hatch distance, scanning speed, and laser beam spot size processing parameters. It is defined as surface or volumetric according to the part geometry. It is derived as a surface for thin-walled structures and volumetrically for solid and high-walled parts. The volumetric energy density is calculated as seen in Equation 3 with its units [23].

$$\boldsymbol{VED_H}\left(\frac{\boldsymbol{J}}{\boldsymbol{mm^3}}\right) = \frac{\boldsymbol{Laser\ power}}{\boldsymbol{Build\ rate}} = \frac{\boldsymbol{P\ (Watt)}}{\boldsymbol{V}\left(\frac{\boldsymbol{mm}}{\boldsymbol{s}}\right)\boldsymbol{.H\ (mm).L\ (mm)}} \qquad (3)$$

Where, VED_H is the volumetric energy density, P is the laser power, V is the average scanning speed, H is the hatch distance, L is the layer thickness parameters.

Except for the scanning strategy, all machining parameters were kept equal in the parts manufactured in scope of the study. By substituting the processing parameters from **Hata! Başvuru kaynağı bulunamadı.** into the calculation in Equation 3, the volumetric energy density values for both scanning techniques were calculated to be 67.3 (j/mm^3). Yakout et al., in their study with Invar 36, examined the melt pool with a high-speed thermal camera in order to reveal the formation of spatter agglomeration and delamination [10]. In the scope of the investigation, samples with different volumetric energy densities were compared with the bidirectional SSS. In contrast to Yakout et al. research, the volumetric energy density was kept constant for the duration of this investigation. In this investigation, the parameter for the scanning strategy, which does not affect the volumetric energy density, was used as a variable, and two distinct manufacturing procedures were used. Examined were the impacts of the CSS, which separates the regions of energy input into islets and not as a line (SSS). In the research by DebRoy et al., the decrease of scan area size is one of the recommended strategies for reducing the influence of residual stresses [14]. Remember that residual stresses are one of the primary causes of delamination [13], [23].

3.2. Density Measurement And Porosity Ratio

The findings of density and porosity measurements using the Archimedes principle are listed in Table 2. Two measurements were performed for each sample. To determine the influence of various scanning procedures on porosity [24], measurements were conducted under the same laser energy density.

Lathe-cut samples collected from the bottom, middle, and higher layers were used to analyze the outcomes. Consequently, the porosity ratio of SSS samples from the bottom layer and middle layer is 6% and 20% greater than that of CSS samples, respectively. In the upper layer, the porosity value of the SSS sample was determined to be 2.84 times that of the CSS sample. This difference in the top layer samples is an indication that the fusion problems become more pronounced as the delamination zone approaches.

Table 2. The density and porosity ratio results for each building strategies using Archimedes' principle (#: sample number / measurement number, E=0,9990 g/cm3 @16°)

	A (g)	F (g)	D (g/cm^3)	f (%)	Fullness (%)	Avg f (%)
#			SSS			
1/1	2,0359	1,7597	7,3637	7,9533	92,0467	**7,972**
1/2	2,0358	1,7595	7,3607	7,9911	92,0089	
2/1	2,7461	2,3926	7,7605	2,9931	97,0069	**3,003**
2/2	2,7463	2,3927	7,7589	3,0135	96,9865	
3/1	7,8902	6,8738	7,7551	3,0609	96,9391	**3,194**
3/2	7,8902	6,871	7,7338	3,3272	96,6728	
#			CSS			
1/1	5,9246	5,1633	7,7744	2,8196	97,1804	**2,807**
1/2	5,9246	5,1635	7,7765	2,7941	97,2059	
2/1	5,8207	5,0747	7,7947	2,5657	97,4343	**2,542**
2/2	5,8204	5,0748	7,7985	2,5184	97,4816	
3/1	7,9406	6,9141	7,7279	3,4016	96,5984	**3,395**
3/2	7,9402	6,9139	7,7290	3,3877	96,6123	

In the CSS part, the porosity values of the sample obtained from the upper layer are seen to increase by 10% compared to the ones in the middle layer. Since the difference is small in comparison to the values obtained in the SSS part, it is difficult to conclude that the delamination in the CSS part is a result of the change in porosity. Moreover, the porosity of the lower layers is greater than the upper layers, however delamination did not occur in the lower layers.

In light of the aforementioned results, it is evident that the porosity ratio changes in the build direction are better with CSS than with SSS. However, its impact on delamination is controversial.

3.3. Tensile Test

Table 3 provides a summary of the numerical values of the tensile test equipment outputs, which are shown graphically in Figure 11. Where; σy represents the yield stress, σuts represents the tensile stress, and %δ represents the percentage of elongation.

Table 3. Tensile test results for all sample types

	σ_y (MPa)	σ_{uts} (MPa)	L_u (mm)	%δ
Stripe_1	624	695	34,7	15,7
Stripe_2	604	687	35,1	17,0
Chess_1	629	714	38,0	26,7
Chess_2	673	755	37,4	24,7

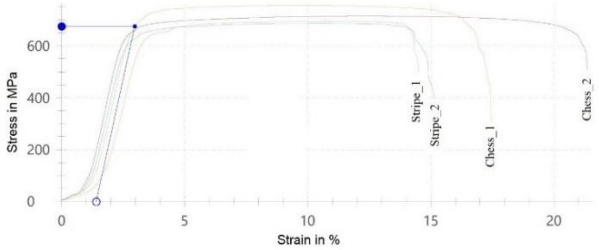

Figure 11. Each sample type's tensile test equipment outputs

According to the results of tensile tests, the yield-tensile strength and elongation rates of samples made from CSS are higher than those made from SSS. Reference yield stress values for the material made by EOS Company, 316L powder with a 40 µm layer thickness are 480 MPa in the building direction and 540 MPa in the horizontal manufacturing direction tensile direction [22]. 540 MPa is the comparison value when building direction of the test specimens are considered. The end result of the test was slightly greater than the reference value. Using the reference value in the analysis and calculations to be performed during the design of the caliper will result in an extra safety factor of 1.1.

Figure 12. As a result of the tensile test, samples that rapture

Figure 12 depicts specimens that have fractured as a consequence of the tensile test. It can be seen from these images that the fractures are ductile. When both methods are compared, according to the tensile test results, the fact that the elongation value of CSS is approximately 50% higher can be seen from the sample images.

3.4. Brinell Hardness Test

In the context of the research, the Brinell hardness test was conducted on two samples manufactured using both scanning strategies. 187,5 kgf (HBW 2,5/187,5) was applied to 316L samples manufactured of SLM with a 2,5 mm diameter ball within the scope of the experiment. Figure 13 presents photos of the two sample types measured for Brinell hardness in the scope of the research. The measurement results for the locations numbered in Figure 13 on each sample surface are given in Table 4.

Table 4. Brinell hardness test results from measurement points for each sample

Scanning strategy	Hardness symbol	HBW 1	HBW 2	HBW 3
SSS specimen	HBW 2,5/187,5	186	196	157
CSS specimen	HBW 2,5/187,5	213	215	-

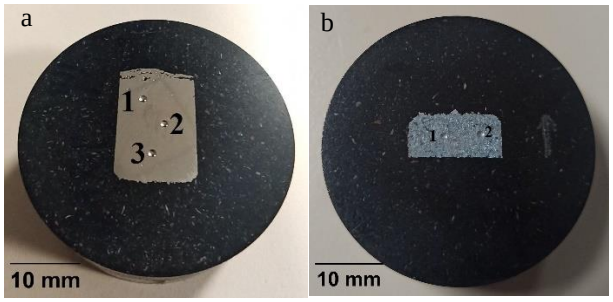

Figure 13. Brinell hardness measurement samples; (a) SSS, (b) CSS

According to the results, CSS provides 10-15% higher hardness outcomes compared to SSS.

3.5. Vickers Hardness Test

As shown in Figure 14 and Figure 15, Vickers low force hardness measurements were performed on samples manufactured with both SSS and CSS (Figure 13) scanning techniques, in three series from the bottom layer to the top layer at 0.5 mm intervals from the plane perpendicular to the building surface.

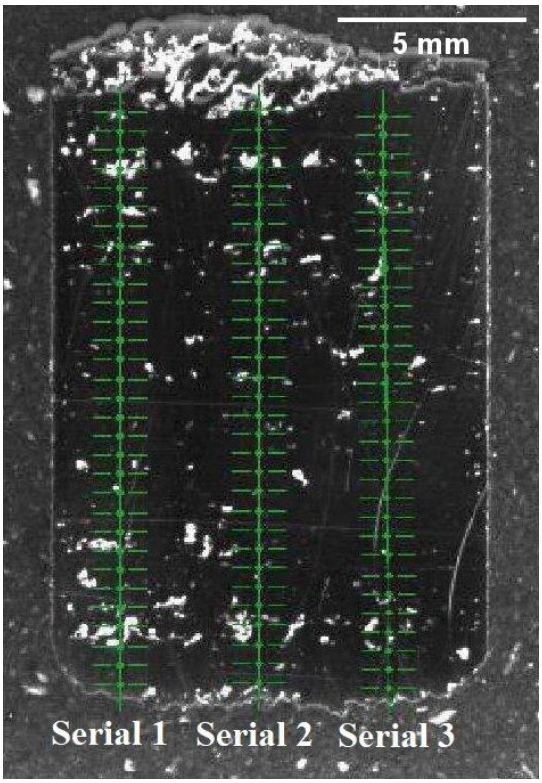

Figure 14. Vickers hardness test measurement series and points for SSS sample

Şekil 9. Maksimum Equivalent Stress Theory'ye göre emniyet katsayısı (S) (Safety factor (S) according to Maximum Equivalent Stress Theory)

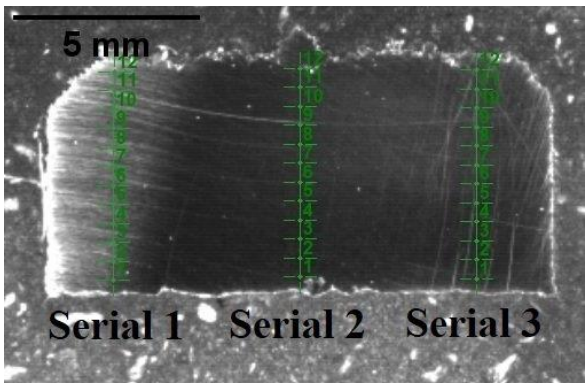

Figure 15. Vickers hardness test measurement series and points for CSS sample

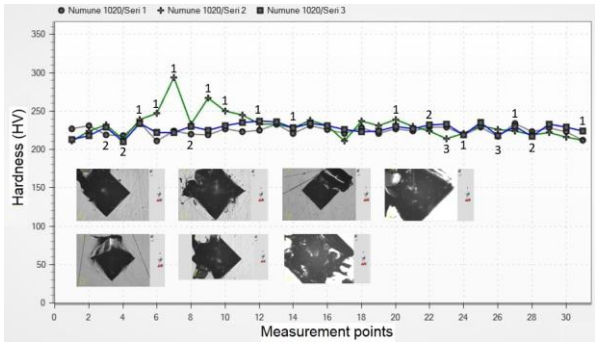

Figure 16. Vickers hardness test measurement results for SSS sample

Figure 16 and Figure 17 illustrates Vickers hardness values based on measurement points and series. On several measurement points in the illustrations, the numbers 1-3 correspond to the wrong measurement point numbers on the same horizontal axis. Figure 16 depicts the SSS sample measurement graph with Vickers hardness values from a total of 93 measurement points. 27 of these measurements cannot be obtained accurately because the indenter overlaps with the void. In the SSS sample, inaccurate measurements were changed with values obtained from the closest region, which appeared to be void-free in the horizontal direction. An example of this situation is seen in Figure 18. One side of the square shaped trace left by the Vickers indenter is approximately 60 µm. Figure 16 shows distorted indenter traces at problematic measurement points. Figure 17 of the CSS sample shows that the indenter impacted the void region in 4 of 39 measurements. In other words, the Vickers indenter coincides with the voids in 29% of the measurements from the SSS sample and 10% of the measurements from the CSS sample. The reason for this difference is that the fusion gaps in the SSS sample are higher than the CSS. The white spots seen on the sample surface in Figure 14 and Figure 15 are lack of fusion voids. These voids on the CSS sample surface, as seen in Figure 15, are substantially smaller and less numerous than those on the SSS one.

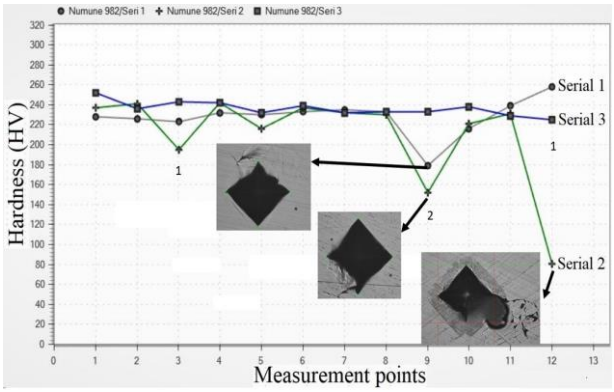

Figure 17. Vickers hardness test measurement results for CSS sample

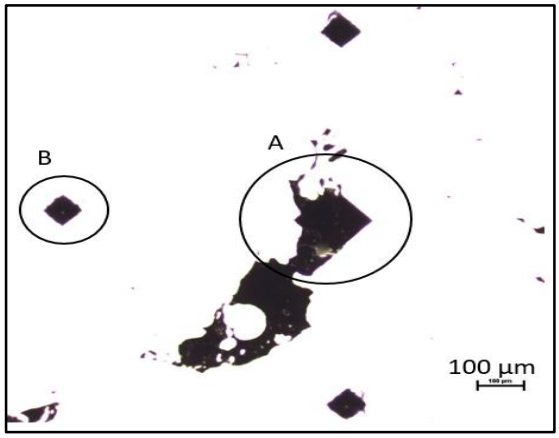

Figure 18. In the SSS sample, the inaccurate measuring point (A) and the shifted measuring point from the void-free zone in the same layer (B)

The obtained Vickers measurement results indicated that the Vickers hardness test is unsuitable for SLM-manufactured components with a high probability of fusion voids. The Brinell hardness measurement technique, which exerts force with a ball on a larger surface than the Vickers indenter, is more suitable for measuring the hardness of SLM-manufactured components.

According to Vickers measurements obtained from the void-free zones, the stiffness is independent of the layer height. Even in the upper layers where delamination was observed, large deviations in values were not observed. When the four defective points recorded in the CSS sample were excluded from the average, the Vickers measurement result averaged 233.6 HV. Similarly, the average Vickers measurement value was calculated to be 226.4 HV when the two defective points detected during the measurement of the SSS sample were excluded from the average. The difference between CSS and SSS hardness measurements is about 3.2%. Due to the inclusion of void effects in the hardness measurement using a large surface spherical indenter, Brinell's results differed by 15%.

3.6. Optical Microscope Examinations

The samples seen in Figure 19a and b, which was produced using SSS and CSS, was subjected to microscopy imaging.

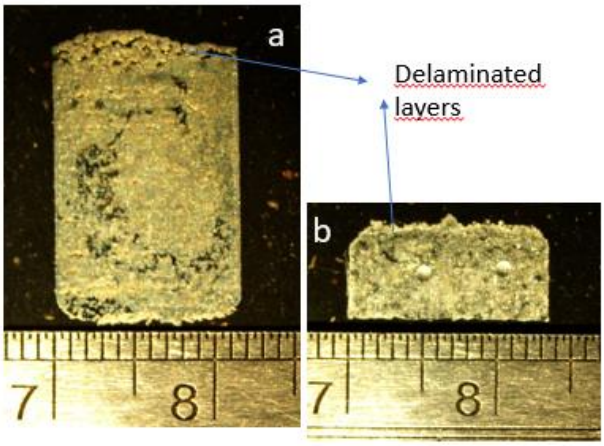

Figure 19. Surface etched SSS (a) and CSS (b) samples

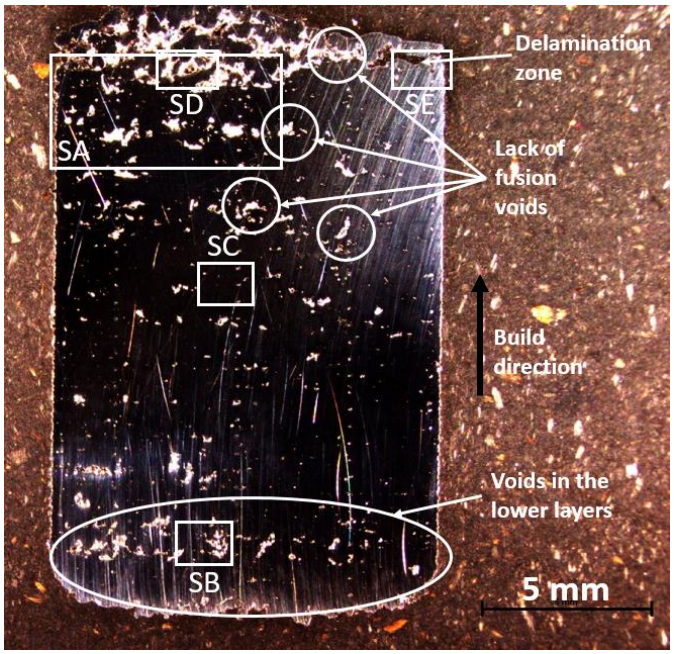

Figure 20. Optical microscope image of SSS sample

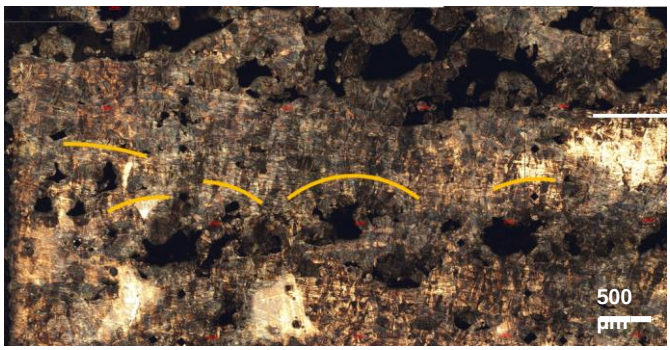

Figure 21. Region SA made up of sixteen 50X photos combined

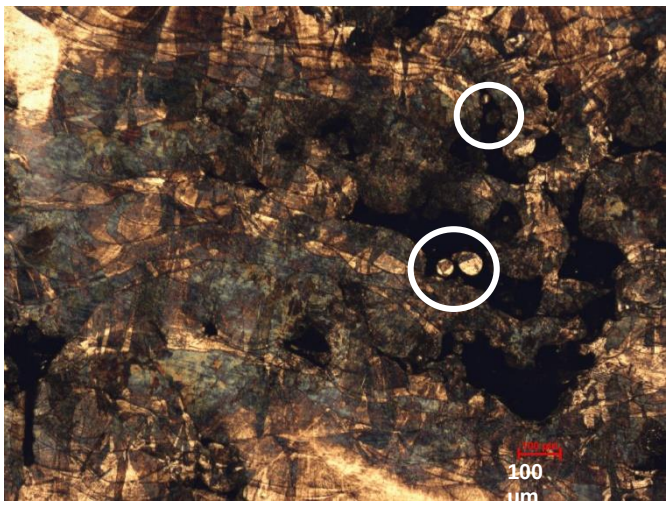

Figure 22. SSS sample; 50X magnification microscopy image of region SB as described in Figure 20

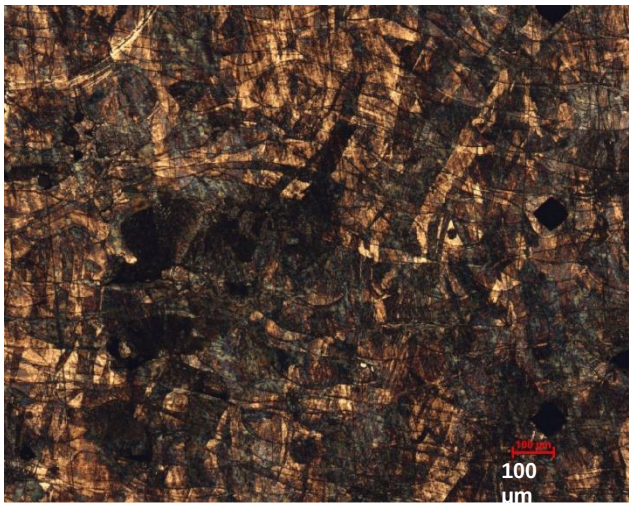

Figure 23. SSS sample; 50X magnification microscopy image of region SC as described in Figure 20

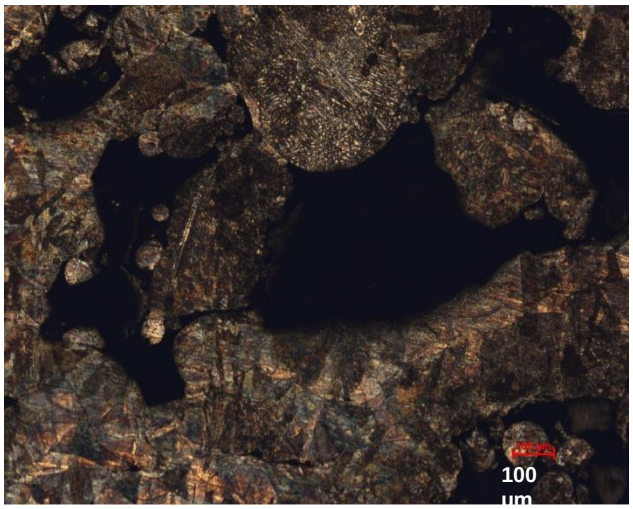

Figure 24. SSS sample; 50X magnification microscopy image of region SD as described in Figure 20

Figure 25. SSS sample; 50X magnification microscopy image of region SE as described in Figure 20

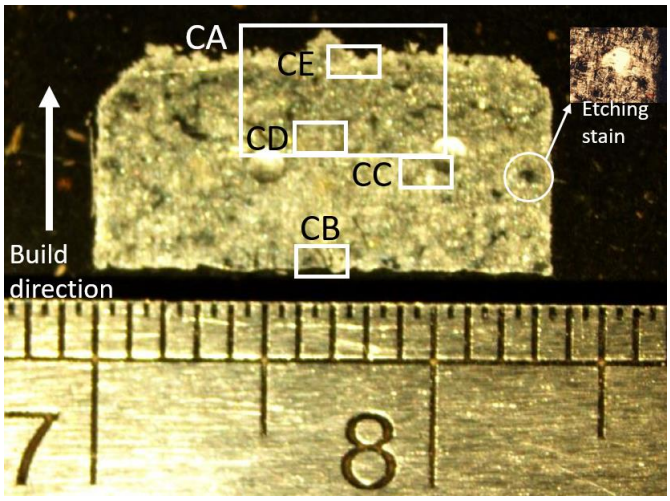

Figure 26. Etched surface image of CSS sample

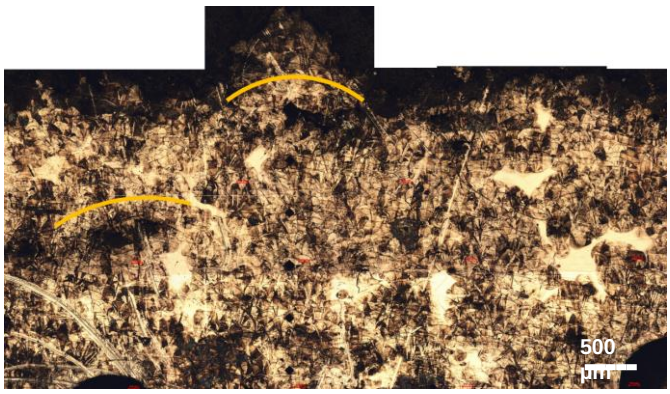

Figure 27. Region CA made up of fifteen 50X photos combined

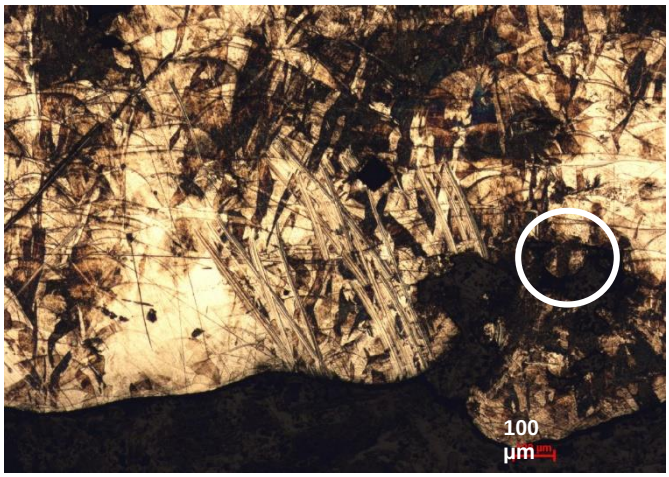

Figure 28. CSS sample; 50X magnification microscopy image of region CB as described in Figure 26

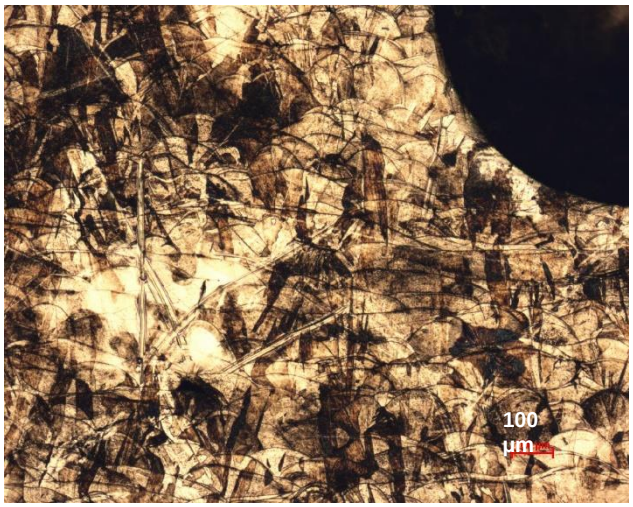

Figure 29. CSS sample; 50X magnification microscopy image of region CC as described in Figure 26

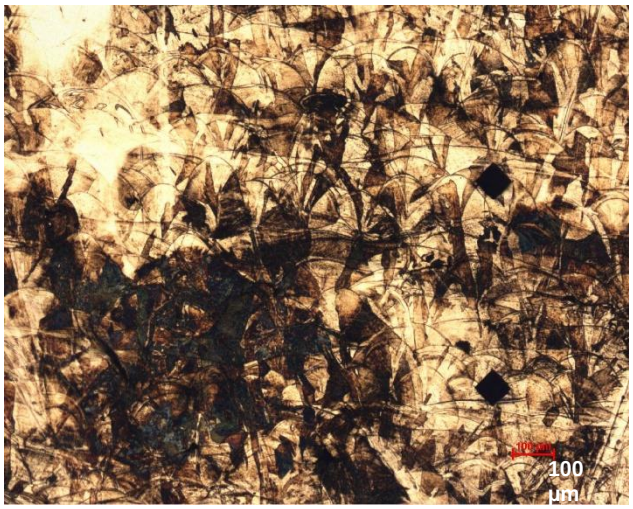

Figure 30. CSS sample; 50X magnification microscopy image of region CD as described in Figure 26

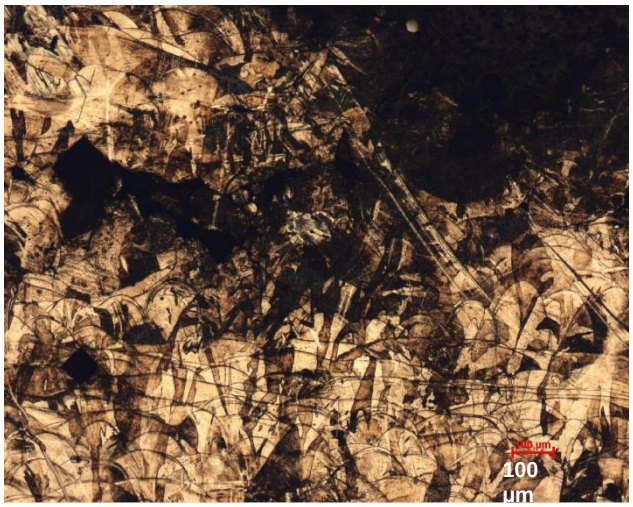

Figure 31. CSS sample; 50X magnification microscopy image of region CE as described in Figure 26

Figure 21 depicts the picture acquired from the SA area of the SSS sample, which was constructed by merging 16 photos. Yellow lines emphasize the distortions and swellings induced by the fusion gaps bigger than 0.5 mm therefore in layer development. Figure 27 depicts similar structures in the CA zone of the CSS sample, which has less porosity than the SSS sample. Yellow lines depict the defects in the layers laid after the voids of between 0.3 and 0.7 mm. The powders deposited after the layers with voids were laid over rough surfaces may have conveyed the swellings to the top layers. In their investigation of the persistence of a substrate problem, Gao et al. reached the conclusion that the substrate error is persistent and cannot be repaired with heat treatments. Additionally, the cooled surface acts as a substrate for the freshly deposited powder [25]. For both samples, in the detail photographs taken from the lower layers in Figure 22 and Figure 28, unmelted powders are seen in thelarge-sized voids. Unmelted powders are shown in the white circle.

Detail photos of the middle layer are shown in Figure 23 for the SSS sample, and in Figure 29 and Figure 30 for the CSS sample. It is seen that the microstructures seen in these images show a regular distribution compared to the lower and upper layers. For the SSS sample, it was observed that the number of voids was relatively low in the images taken from the middle layer. At 50X magnification, very few voids smaller than 50 µm were seen in the CSS sample.

For both samples, the upper layers are the regions where delamination begins. Figure 24 and Figure 25 include detailed photographs of the SSS sample, whereas Figure 31 depicts the CSS sample. Specifically, in Figure 25 from the SSS sample, the delamination is visible on the fabricated part's outside surface.

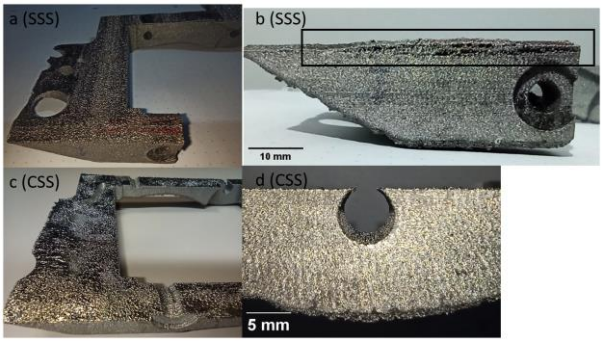

Figure 32. Surface lacking in dimensional accuracy (a,c), delamination surface on the top surface of the part (b,d)

The surfaces seen in Figure 32a and c are the photographs taken with an angle view to Figure 3a and b. Although CSS reduced delamination, fabrication still failed due to delamination.

4. CONCLUSION

This study aims to compare the impacts of stripe and chessboard scanning strategies on mechanical characteristics and delamination, while keeping a

constant VEDH value. In this context, density tests, determination of porosity, tensile test and hardness measurements, and microscopic examinations were conducted for both scanning strategies. Consequently, the findings and future researches can be seen below:

- Samples from the bottom, middle, and top layers of the manufactured components were examined for density. Density and, thus, porosity measurements differed with layers. This variation in values is higher in SSS samples than in CSS samples. The porosity ratio of the sample collected from the upper levels of the SSS component was found to be 2.8 times that of the sample taken from the same layer of the CSS.
- Depending on the layer height, the CSS part's porosity value ranges between 10% and 33%. This ratio increases from 6% in the lower layers to 265% in the upper layers of the SSS.
- In the tensile test, the average yield strength of CSS was 6% greater than that of SSS. In addition, CSS exhibited greater ductility and 1.5 times the elongation rate of SSS. Although delamination occurred during fabrication, the yield strength of the samples produced was roughly 10% greater than the properties of the reference material.
- It was difficult to get a Vickers measurement because to the severe porosity. In the SSS sample in particular, 27 of the 93 measurement points were repeated in order to get the void-free areas. The filled regions exhibit a minor change in measurement values throughout the layer height, including the delamination zone. The filled region measurement findings showed that the CSS sample had 233.6 HV and the SSS sample 226.4 HV.
- In comparison to the Brinell measurement, the CSS hardness levels were, on average, 12 percent greater. Because the Brinell indenter is bigger than the Vickers indenter, porosity is included into the measurement, resulting in a larger difference in Brinell measurement findings.
- According to microstructure examinations, the significant (0.5-0.7 mm) voids in the higher layers were associated with the delamination that had occurred. In order to reveal the causes of void formation, the behavior of the melt pool can be observed with a more detailed experimental setup using a high speed thermal camera.
- Manufacturing should be repeated using a chessboard scanning strategy developed by decreasing the islet area's value. With different VEDH values, more samples could be manufactured and examined simultaneously.

ACKNOWLEDGEMENT

This work was funded and supported by the FNSS - Savunma Sistemleri A.Ş.

DECLARATION OF ETHICAL STANDARDS

The authors declare that they have no known competing financial interests or personal relationships that could have appeared to influence the work reported in this paper.

AUTHORS' CONTRIBUTIONS

Mehmet Özakıncı: Conceptualization, Methodology, Investigation, Writing – original draft, Visualization, Funding acquisition.

Rahmi Ünal: Conceptualization, Writing – review & editing, Supervision..

CONFLICT OF INTEREST

The authors declare that there is no conflict of interest regarding the publication of this paper.

REFERENCES

[1] Yalçın B., Karakılınç U., and Ergene B., "Toz Yataklı/Beslemeli Eklemeli İmalatta Kullanılan Partiküllerin Uygunluk Araştırması ve Partikül İmalat Yöntemleri", ***J. Polytech.***, 22(4): 801–810, (2019).

[2] Kayacan M. Y. and Yılmaz N., "DMLS Eklemeli İmalatta Süreç Ve Maliyet Modeli Geliştirilmesi", ***J. Polytech.***, 22(3): 763-770, (2019).

[3] Balcı A., Aycan M. F., Usta Y. and Demir T., "Seçimli Lazer Ergitme İle Ti6Al4V ELI Alaşımından Üretilen Trabeküler Metal Yapıların Basma Ve Basma-Kayma Dayanımlarının İncelenmesi", ***J. Polytech.***, 24(3): 903-914, (2021).

[4] Yampolskiy M. *et al.*, "Security of additive manufacturing: Attack taxonomy and survey", ***Addit. Manuf.***, 21: 431–457, (2018).

[5] Mugwagwa L., Yadroitsev I., and Matope S., "Effect of process parameters on residual stresses, distortions, and porosity in selective laser melting of maraging steel 300", ***Metals***, 9(10): 1042, (2019).

[6] Ponticelli G. S., Panciroli R., Venettacci S., Tagliaferri F., and Guarino S., "Experimental investigation on the fatigue behavior of laser powder bed fused 316L stainless steel", ***CIRP J. Manuf. Sci. Technol.***, 38: 787–800, (2022).

[7] Röttger A. *et al.*, "Microstructure and mechanical properties of 316L austenitic stainless steel processed by different SLM devices", ***Int. J. Adv. Manuf. Technol.***, 108(3): 769–783, (2020).

[8] Moeinfar K., Khodabakhshi F., Kashani-bozorg S. F., Mohammadi M., and Gerlich A. P., "A review on metallurgical aspects of laser additive manufacturing (LAM): Stainless steels, nickel superalloys, and titanium alloys", ***J. Mater. Res. Technol.***, 16: 1029–1068, (2022).

[9] Carter L. N., Attallah M. M., and Reed R. C., "Laser powder bed fabrication of nickel-base superalloys: Influence of parameters; characterisation, quantification and mitigation of cracking", ***Proc. Int. Symp. Superalloys***, Pennsylvania, 577–586, (2012).

[10] Yakout M., Phillips I., Elbestawi M. A., and Fang Q.,

"In-situ monitoring and detection of spatter agglomeration and delamination during laser-based powder bed fusion of Invar 36", ***Opt. Laser Technol.***, 136: 106741, (2021).

[11] Qiu C., Al Kindi M., Aladawi A. S., and Al Hatmi I., "A comprehensive study on microstructure and tensile behaviour of a selectively laser melted stainless steel", ***Sci. Rep.***, 8(1): 1–16, (2018).

[12] Liverani E., Toschi S., Ceschini L., and Fortunato A., "Effect of selective laser melting (SLM) process parameters on microstructure and mechanical properties of 316L austenitic stainless steel", ***J. Mater. Process. Technol.***, 249: 255–263, (2017).

[13] Kempen K., Vrancken B., Buls S., Thijs L., Van Humbeeck J., and Kruth J. P., "Selective Laser Melting of Crack-Free High Density M2 High Speed Steel Parts by Baseplate Preheating", ***J. Manuf. Sci. Eng. Trans. ASME***, 136(6): 1–7, (2014).

[14] DebRoy T. *et al.*, "Additive manufacturing of metallic components – Process, structure and properties", ***Prog. Mater. Sci.***, 92: 112–224, (2018).

[15] ASTM E8/E8M-22, "Standard Test Methods for Tension Testing of Metallic Materials", (2022).

[16] Öz Ö. and Öztürk F. H., "Yazdırma Açısının 3B Yazıcıda Üretilen PLA Numunenin Mekanik Özellikleri Üzerine Etkisinin Deneysel ve Sonlu Elemanlar Metodu ile İncelenmesi", ***J. Polytech.***, 1-1, (2023).

[17] ISO 6507-1, "Metallic materials - Vickers hardness test - Part 1: Test method", (2018).

[18] ASTM B311-22, "Standard Test Method for Density of Powder Metallurgy (PM) Materials Containing Less Than Two Percent Porosity", (2022).

[19] Tüzemen M. Ç., Salamcı E., and Ünal R., "Investigation of the relationship between flexural modulus of elasticity and functionally graded porous structures manufactured by AM", ***Mater. Today Commun.***, 31: 103592, (2022).

[20] Tüzemen M. Ç., Salamcı E., and Ünal R., "Additive manufacturing design approach to strut-based functionally graded porous structures for personalized implants", ***J. Manuf. Process.***, 84: 1526–1540, (2022).

[21] Taylor R. P., McClain S. T., and Berry J. T., "Uncertainty analysis of metal-casting porosity measurements using Archimedes' principle", ***Int. J. Cast Met. Res.***, 11:4, 247-257, (1999).

[22] **https://matweb.com,** "MatWeb Material Property Data," *AISI Type 316L Stainless Steel, annealed bar*. Available: (Accessed: 03-Nov-2022).

[23] Kurzynowski T., Stopyra W., Gruber K., Ziólkowski G., Kuznicka B., and Chlebus E., "Effect of scanning and support strategies on relative density of SLM-ed H13 steel in relation to specimen size", ***Materials (Basel).***, 12(2): 239, (2019).

[24] Dursun A. M., Tüzemen M. Ç., Salamci E., Yılmaz O. and Ünal R., "Investigation of Compatibility Between Design and Additively Manufactured Parts of Functionally Graded Porous Structures", ***J. Polytech.***, 25(3): 1069-1082, (2022).

[25] Gao M., Wang Z., Li X., and Zeng X., "The effect of deposition patterns on the deformation of substrates during direct laser fabrication", ***J. Eng. Mater. Technol.***, 135(3): 034502, (2013).